

Probing precise interatomic potentials by nonadiabatic nonlinear phonons

Shi-Qi Hu^{a,b}, Da-Qiang Chen^{a,b}, Sheng-Jie Zhang^{a,b}, Xin-Bao Liu^{a,b}, Sheng Meng^{a,b,c,*}

^a National Laboratory for Condensed Matter Physics and Institute of Physics, Chinese Academy of Sciences, Beijing, 100190, PR China

^b School of Physical Sciences, University of Chinese Academy of Sciences, Beijing, 100049, PR China

^c Songshan Lake Materials Laboratory, Dongguan, Guangdong, 523808, PR China

ABSTRACT

Accurately probing the interatomic potential (IP) in crystals is essential for understanding the dynamic mechanisms in phase transitions and chemical reactions. Here, by interrogating laser-induced coherent phonon dynamics, we propose a new kind of optical microscopy for determining effective interatomic potentials beyond the harmonic and adiabatic approximation. This technique is tested against available experimental and first-principles data, by which the interatomic potential of graphene and a few other materials are successfully reconstructed in a large configuration space and beyond the ground state. A significant nonadiabatic effect emerges in nonlinear phonon dynamics and the IP reconstruction, which corrects the anharmonic part of IP much stronger (up to 50%) than the harmonic part. The nonadiabaticity-modulated potentials can lead to $\sim 10\%$ correction on thermal expansion coefficients and ~ 0.3 eV on phase transition barriers. This work offers a new strategy for probing complex interactions in quantum materials and exemplifies the universality of nonadiabaticity, which deserves a full consideration for precisely determining physical properties of quantum many-body systems.

The interatomic potential (IP) describes the internal interactions and creates a smooth energy “landscape” for atomic motions, where the dynamic process can be viewed from a topology perspective. Therefore, accurate and complete determination of the interaction potential plays a central role in many dynamic processes including the phase transitions among ferroelectricity, superconductivity or charge density waves (CDW) phase [1–6], and the proton-coupled electron transfer which governs biological reactions such as vision [7].

One of the standard ways to characterize the IP is the potential energy surface (PES), which describes the potential energy of a system, i.e., a collection of atoms, in terms of certain geometric parameters, typically the positions of the atoms [8,9]. However, the PES concept is usually based on the adiabatic Born-Oppenheimer (ABO) approximation [10, 11]. When the energy gap between electronic states is close to the energy scale of the nuclear motions, the feedback between electronic transitions and atomic motions become significant. This feedback modulates the effective IP to be the combination of potential configurations in the ground state and various excited states. Therefore, the PES within ABO approximation fails for an accurate description of IP and atomic dynamics [12]. A broad range of previous studies have revealed the effects of nonadiabaticity on the phonon frequency by renormalizing the phonon self-energy [13,14]. The results imply that the IP in electron-phonon interaction dominated materials has significant nonadiabatic (NA) effects [15,16], where the ground-state PES is inadequate.

These studies are mainly based on the harmonic potential approximation of IP, whereas the higher-order nonlinear contributions are usually ignored. This approximation works well for the thermal equilibrium phonons (TEPs), which originate from the thermal excitation and vibrate with a small amplitude [17,18]. Nevertheless, the harmonic assumption limits the accurate description of IP in a small geometry space near the equilibrium atomic positions. With the rapid development of nonlinear optics especially the terahertz technologies [19], probing and controlling the atomic dynamic far from equilibrium, such as the generation of strong nonlinear coherent phonons (SNCPs), have been routinely achieved nowadays [20–22]. For the SNCPs which are excited by laser pulse, the atomic displacements spread a very large space scale and introduce a strong phonon nonlinearity, so that the harmonic approximation is insufficient. Indeed, many previous studies have shown the breakdown of harmonic IP in describing interatomic interactions, as exhibited in the thermal conductivity [23–25] and ultrafast lattice relaxation [22,26–28]. In order to understand and control the dynamics out of equilibrium reliably, as well as the related material properties, clarifying the NA effects on nonlinear contributions of IP is urgently needed. Unfortunately, such efforts remain elusive.

In this article, we explore the excited-state coherent phonon dynamics and based on that an all-optical IP probing is developed. The technique enables us to reconstruct an effective IP without harmonic and adiabatic approximation and beyond the ground-state PES, with the phonon oscillation spectra (POS) for both symmetry-maintaining and

* Corresponding author. National Laboratory for Condensed Matter Physics and Institute of Physics, Chinese Academy of Sciences, Beijing, 100190, PR China.
E-mail address: smeng@iphy.ac.cn (S. Meng).

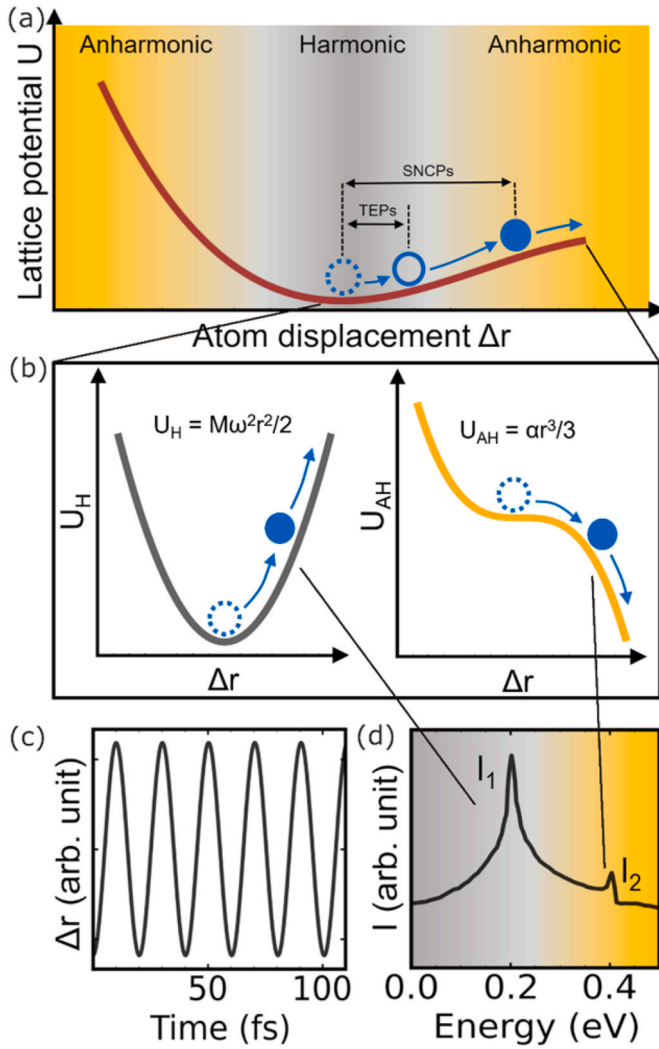


Fig. 1. (a) The interatomic potential U as a function of phonon amplitude Δr . The grey and yellow regions schematic the harmonic and anharmonic ranges of U . The blue circles and arrows describe the atom and its oscillation in the interatomic potential. The black arrows label the atom motions of thermal equilibrium phonons (TEPs, open circle) and strong nonlinear coherent phonons (SNCPs, solid circle), respectively. (b) The harmonic (U_H , grey line) and anharmonic (U_{AH} , yellow line) part of U as a function of phonon amplitude Δr . (c) The phonon amplitude Δr as a function of time. (d) The phonon oscillation spectra (POS) obtained by the Fourier transform of (c). The grey and yellow regions label the harmonic (I_1) and anharmonic (I_2) phonon peaks originating from the atom scattering by U_H and U_{AH} of (b).

symmetry-breaking phonons, which can be obtained by the pump-probe measurements [29–35] as the only input. We note that von Hoegen et al. achieved probing the total IP of symmetry-breaking phonon with the strong-field nonlinear phononics [36], based on the second-harmonic spectra. A significant NA effect has been revealed in nonlinear phonon dynamics and the IP probing, which can strongly affect the nonlinear (anharmonic) parts of IP (up to 50%) in graphene and a few other quantum materials. As the physical consequences, the probing of phonon-mode-resolved Young's modulus, thermal expansion coefficient (TEC) and phase transition barriers are also corrected by NA effects, esp. for systems out of equilibrium. Since the above properties are vital for phase transition and reaction process such as the emergence of CDWs [37–40] and single-atom catalysts [41–46], fully considering the NA effects on nonlinear interaction and dynamics are essential for both fundamental science and real applications including photoelectronic devices and renewable energy applications.

The investigations are performed with the state-of-the-art first-principles calculations. The phonon dynamics are introduced by an initial stretch of the bond between atoms along the phonon eigenmode displacement. (For TEPs the atom displacement u_0 is $\sim 0.5\%$ of the equilibrium bond length a_{C-C} , corresponding to the phonon amplitude under ~ 30 K temperature. While for SNCPs the stretch is $u_0 \sim 2\%$ of a_{C-C} .) The adiabatic phonon dynamics are simulated by the ground state molecular dynamics (MD). While the NA dynamics are realized by considering the interaction between the electrons and atoms and evolving both of them simultaneously, based on real-time time-dependent density-functional theory molecular dynamics (rt-TDDFT-MD) [47–49]. To quantify the phonon dynamics nonlinearity and to reconstruct the effective IP, the POS are obtained by the Fourier transform of the phonon vibration as a function of time, from simulations and available experiments. The structures and IP energies are obtained from the adiabatic and NA MD simulations, respectively. The potential difference between them is defined as the NA correction. The IP with NA corrections can be understood by the dominant Coulomb interaction $Z_R \int \frac{n'(r)}{|r-R|} dr$ between atoms (ions) and nonequilibrium distributed electrons due to the NA effects, where the nonequilibrium electron distribution $n'(r)$ is obtained by self-consistently solving the time-dependent Kohn-Sham equation within the coherent phonon bath, based on the TDDFT. More details about the method can be found in the supplementary materials [50].

1. The nonlinear phonon dynamics and IP probing

Similar to the picoscopy of valence electrons in solids [51], the phonon dynamics can be understood within the framework of scattering theory [52,53]. As shown in Fig. 1(a), here we consider only the lowest order nonlinear term of IP (as shown in Fig. S6 [50], in the phonon amplitude range of our study, the lowest order term is sufficient to describe the anharmonic feather of IP), and thus the global effective IP (represented by U) has the form:

$$U = m\omega^2 r^2/2 - \alpha r^3/3 \quad (1)$$

which is composed by the harmonic part $U_H = m\omega^2 r^2/2$ and anharmonic component $U_{AH} = \alpha r^3/3$ (Fig. 1(b)). ω is the phonon frequency in U_H and α is the anharmonic coefficient in U_{AH} . The atoms oscillate at frequency ω in the lattice potential and form the collective mode, i.e., the phonons. During the oscillation, the atoms are scattered by the IP, which in turn modulates the phonon motions and the POS structure (Fig. 1(c–d)). The scattering process means that the atom motions are determined by the IP through the Newton equation: $\partial^2 r(t)/\partial t^2 = -\partial U/\partial r(t)$, where $r(t)$ is the atom displacement of coherent phonons oscillating with time and $U = m\omega^2 r^2/2 - \alpha r^3/3$ is the IP corresponding to the phonons. Since the IP includes both the harmonic part $U_H = m\omega^2 r^2/2$ and anharmonic component $U_{AH} = \alpha r^3/3$, $r(t)$ is mainly contributed by two parts: $r(t) = r_h(t) + r_v(t)$, $r_h(t) = r_0 \cos(\omega t)$ is the dominant oscillation with phonon frequency ω , whose driving force comes from the U_H . While $r_v(t)$ is the nonlinear oscillation resulting from the driving force contributed by the anharmonic IP part U_{AH} [50]. For TEPs, the atom displacement is near the equilibrium position and thus the harmonic potential scattering is dominant. While for SNCPs, the atoms go into the anharmonic region, the scatterings by the anharmonic potential become significant. The anharmonic scatterings can yield the high order phonon peaks in POS.

The phonon peak intensity in POS can be derived from the series expansion of Eq. (1). The fundamental (first-order) phonon peak is contributed by the harmonic scattering:

$$I_1 \sim \omega^2 |2\omega^2 \sum (-1)^n J_1(n\pi r_0/l)/(n\pi)|^2, \quad (2)$$

while the second-order phonon peak is mainly contributed by anharmonic scattering:

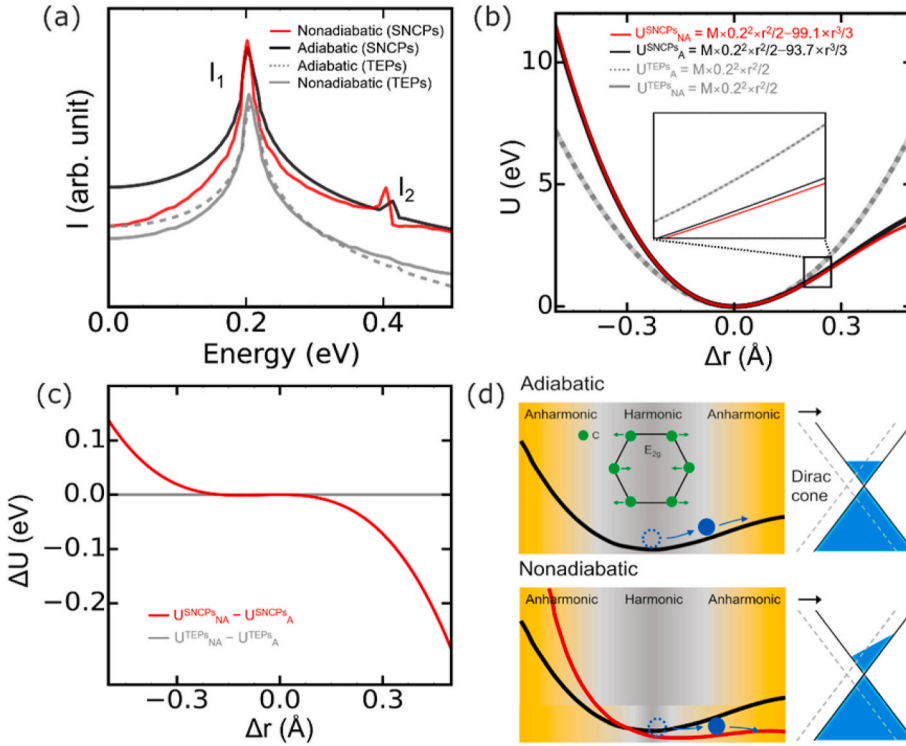


Fig. 2. (a) The phonon oscillation spectra (POS) of SNCPs and TEPs obtained with ABO approximation (adiabatic) and NA corrections (nonadiabatic) in graphene. (b) The interatomic potential U reconstructed from the POS in (a) as a function of phonon amplitude Δr . (c) The energy difference ΔU between interatomic potentials reconstructed from the POS within adiabatic and NA framework. The grey and red lines label the situations of TEPs and SNCPs, respectively. (d) The schematics showing the atom oscillations on the interatomic potential in real space and oscillations of Dirac cone in reciprocal space within adiabatic and NA framework. The solids black and red lines label the interatomic potential with ABO approximation (adiabatic) and NA corrections (nonadiabatic). The grey and yellow regions schematic the harmonic and anharmonic ranges of U . Regions with blue shading on Dirac cone are filled with electrons. The dash grey and solid black lines label the Dirac cones position with atom displacement and the black arrows show the oscillation directions. The inset of (d) shows the real space atomic pattern in the presence of E_{2g} phonon@ Γ in graphene.

$$I_2 \sim 4\omega^2 |2\alpha l^2 \sum (-1)^{n+1} (n^2\pi^2 - 6) J_2(n\pi r_0/l) / (3n^2\pi^2)|^2. \quad (3)$$

Here l is the lattice constant and r_0 is the phonon amplitude. J_1 and J_2 are the first kind Bessel function of order 1 and 2, respectively. The relationship between phonon peak intensity and potential coefficients can be written as:

$$I_1/I_2 = \gamma (\alpha/m\omega^2)^2, \quad (4)$$

where $\gamma = |\omega^2 \Sigma (-1)^n J_1(n\pi r_0/l) / (n\pi)|^2 / |2l^2 \Sigma (-1)^{n+1} (n^2\pi^2 - 6) J_2(n\pi r_0/l) / (3n^2\pi^2)|^2$.

The framework of scattering enables us to reconstruct the effective IP only from the phonon peaks in POS. The harmonic U_H is described by the phonon frequency ω , which can be read directly from the POS. The anharmonic U_{AH} is quantified by the coefficient α , which is obtained from the phonon peak intensity ratio by Eq. (4). By fitting the peak intensity changing with the r_0 , our method can also be extended to probe the IP containing higher order nonlinear terms [50].

The validity of the approach under different field is guaranteed by the parameter γ in Eq. (4), which is also field dependent and thus cancels the field-dependence of I_1/I_2 . As shown in Fig. S10, as the I_1/I_2 changing, the parameter γ also changes accordingly with the strength of field [50]. The ratio between I_1/I_2 and γ is almost constant, guaranteeing the reconstructed $\alpha/m\omega^2$ is stable and field-independent. Since the POS can be detected within a short time scale, the decay of coherent phonon is expected to not affect the IP reconstruction and thus we ignore these processes here.

We first investigate the nonlinear phonon dynamics and IP reconstruction for the dominant E_{2g} phonon@ Γ [13,14] in graphene. Fig. 2(a) plots the POS of TEPs and SNCPs, for both of them, the fundamental phonon peak with frequency $\hbar\omega \approx 0.2$ eV, plays a dominant role in POS. This fundamental phonon peak comes from the linear process of E_{2g} phonon@ Γ which is contributed by the scattering of harmonic potential part U_H . In contrast, for SNCPs there is an additional second-order phonon peak with the frequency $\hbar\omega \approx 0.4$ eV, which originates from the anharmonic scattering by U_{AH} since atoms have larger vibration amplitudes as mentioned before.

Using Eq. (4) we reconstruct the effective IP from the POS of TEPs and SNCPs under ABO approximation and with NA corrections, respectively. As shown in Fig. 2(b) and (c), for TEPs only U_H is probed due to the lack of anharmonic scatterings. For SNCPs, both the harmonic U_H and anharmonic U_{AH} are reconstructed and the IP shows an obvious difference from the parabola, indicating the breakdown of harmonic potential approximation for a large space scale. The phonon frequency ω in harmonic U_H is obtained as $\hbar\omega \sim 0.2$ eV, which is consistent with the experimental value [54–57]. The coefficient α in anharmonic U_{AH} is ~ 93.7 eV/ \AA^3 reconstructed from POS under ABO approximation and ~ 99.1 eV/ \AA^3 with NA effects included. For comparison, we fit the coefficient α directly from the interatomic potential curves with the form $U = m\omega^2 r^2/2 - \alpha r^3/3$ (Fig. S1 [50]). The potential curves describe the energy as a function of different structure configurations, and the different structures and corresponding energies are obtained from the adiabatic and NA MD simulations. The α fitted from the potential-structure curves by adiabatic and NA simulations are ~ 93.4 eV/ \AA^3 and ~ 97.4 eV/ \AA^3 , respectively. The fitting results show good agreements with the reconstructed α from the POS (Fig. S1(b)), demonstrating the self-consistency of our approach.

We also fit the α from experimental measurements [50], which has the value ~ 98.7 eV/ \AA^3 from Lin et al. [56] and ~ 99.8 eV/ \AA^3 from Efthimiopoulos et al. [57]. Since the lack of pump-probe experiment data in graphene blocks us to get the experimental α from I_1/I_2 by Eq. (4), the experimental α in graphene is fitted by the frequency shift as a function of temperature from the Raman spectra measurements [56,57]. We describe the phonons using the classical harmonic oscillator model and treat the anharmonic IP as a perturbation to the harmonic oscillation frequency [50].

We note that the POS in Fig. 2(a) and reconstructed IP in Fig. 2(b–c) show a divergence between adiabatic and NA case (esp. for SNCPs). The results with NA corrections are more consistent with experiment. In fact, this difference indicates that the adiabatic PES is less effective and inaccurate to describe the IP and thus the phonon or phase transition dynamics. Indeed, we estimate that the phase transition energy barrier is overestimated by more than ~ 0.3 eV (~ 3000 K) when the crystal lattice

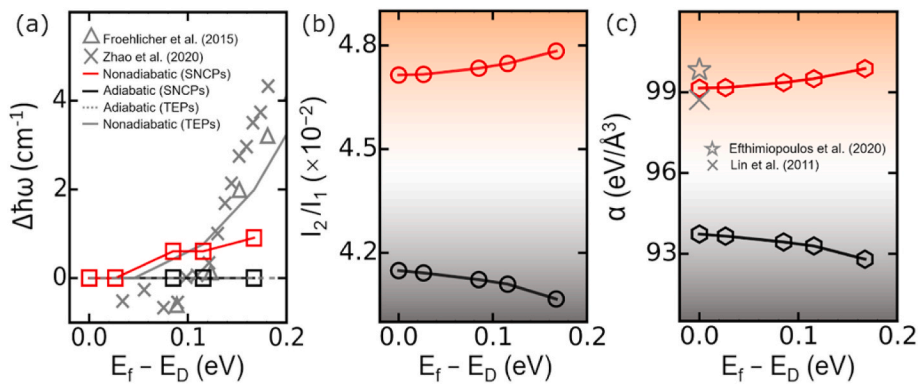


Fig. 3. (a) The evolution of the E_{2g} phonon@ Γ frequency shift $\Delta\omega$ in U_H with doping concentrations (represented by $E_f - E_D$). The grey labels mark the experimental measurements from Zhao et al. [54] and Froehlicher et al. [55], respectively. (b) The intensity ratio between fundamental and second-order phonon peaks in POS, i.e., I_2/I_1 , as a function of doping concentrations. (c) The reconstructed coefficient α of the U_{AH} from the I_2/I_1 of POS in (b) as a function of doping concentrations. The grey labels mark the α fitted from the experimental measurements by Lin et al. [56] and Eftimiopoulos et al. [57]. The black and red colors label the results obtained with ABO approximation (adiabatic) and NA corrections (nonadiabatic), respectively.

melts based on the Lindermann criterion for lattice instability.

Since in the realistic systems, the interatomic interaction in different neighbours has very different values and may affect the phonon dynamics. Here we estimate the neighbour effects by comparing the phonon dynamics obtained from the 1×1 unit cell and the 2×2 supercell which contains the interatomic interaction between different neighbours. As shown in Fig. S9 [50], the phonon dynamics show very similar behaviours in the unit cell and supercell, indicating that the high-order-neighbour effect is less significant in the present case. Another evidence is the doping dependence of phonon energy shown in Fig. 3(a). The results obtained from the unit cell calculations show good agreement with the experimental results, which naturally include the interatomic interactions from different neighbours.

2. The NA effects on nonlinear phonon dynamics and IP

The difference on IP accuracy originates from the lacking of feedback between electron dynamics and atomic motions under ABO approximation. As shown in Fig. 2(d), in graphene the Dirac cones oscillate in the reciprocal space due to the lattice distortion brought by the phonon motions. Within adiabatic framework, the electrons on the Dirac cone move together with the bands and stay in the ground state at any time. The ground state electronic configuration forms a fixed PES where the atoms oscillate in it. Therefore, only the IP within the ABO approximation (the solid black line in Fig. 2(d)) can be described by the ground-state PES. However, considering the NA effects, atomic vibrations lead to transitions between electronic states. The excited electrons have no time to fully relax to the ground state and show a nonequilibrium configuration, which, in turn, alters the potential experienced by the atoms and forms the effective IP (the solid red line in Fig. 2(d)) beyond the ABO approximation. The effective IP can be seen as a combination of ground-state PES and various excited-state PES. Therefore, for an accurate description of IP and dynamics, the NA effects must be considered.

In Fig. 3 we investigate phonon frequency ω , the intensity ratio between fundamental and second-order phonon peaks in POS, i.e., I_2/I_1 , and the anharmonic coefficient α reconstructed from I_2/I_1 as a function of doping concentrations, within adiabatic and nonadiabatic framework. The doping concentration is tuned by adding electrons and described by the Fermi energy shift $E_f - E_D$, where E_f is the Fermi level and E_D is the energy level of Dirac point. For the undoped case, $E_f = E_D$.

The nonadiabaticity in graphene affects the harmonic potential U_H and linear dynamics by the phonon frequency renormalization [13,14,54,55], as shown in Fig. 3(a). The difference of electron configuration between adiabatic and NA framework become more significant with the rise of doping concentration. Due to the enhanced NA effects, the phonon frequency has a blueshift $\Delta\omega$. The $\Delta\omega$ of TEPs shows a good agreement with the experiments [54,55], similar tendency can also be seen for SNCPs while the blueshift becomes smaller, which may result from the phonon nonlinearity caused by anharmonic scatterings.

The nonadiabaticity affects the anharmonic potential U_{AH} and nonlinear phonon dynamics by correcting the anharmonic coefficient α and modulating the nonlinear scattering rate, which is represented by the I_2/I_1 . Compared to the adiabatic case, the value of I_2/I_1 and α with NA corrections shows a large enhancement. Moreover, the doping dependence of I_2/I_1 and α have a completely opposite trend: within the ABO approximation, the I_2/I_1 and α decrease with the doping concentration, while they show an increasing behaviour within the NA framework. The different behaviour of I_2/I_1 implies an improved phonon nonlinearity brought by the nonadiabaticity. The reason can be understood by the prompted α with NA corrections: the nonadiabaticity drives the effective IP away from the harmonic configuration by enhancing the anharmonic contributions. Consequently, there is more anharmonic scattering and the phonon dynamics will be nonlinear.

It is worth to compare the NA effects on the harmonic U_H and anharmonic U_{AH} [50]. The nonadiabaticity is quantified by the ratio between the nonadiabaticity-induced coefficient change and initial coefficient in IP terms (For U_H we use the phonon frequency change $\Delta\omega/\omega$ while for U_{AH} , the $\Delta\alpha/\alpha$ is used.). Taking the doping level at $E_f - E_D \sim 0.17$ eV as an example, NA effect has a 0.06% correction on U_H while a 7.54% correction on U_{AH} , which is more than two orders of magnitudes stronger. The results indicates that by connecting the feedback between electrons and phonon dynamics, the NA effects increase both the harmonic and anharmonic potential in graphene, and the anharmonic potential is more sensitive to NA modulation.

Besides the phonon dynamics, the NA effects also show impacts on the mechanical and thermal properties of materials, by the modulated IP. In Fig. S4, we display the probing on the phonon-mode-resolved Young's modulus and TEC in graphene as a function of doping, based on the IP reconstruction. The results show consistent magnitude with the experimental results [58,59] and indicate that the giant NA effects beyond separate electron and phonon dynamics, which can weak the intrinsic elasticity (by $\sim 2\%$) and increase the thermal expansion coefficient (by $\sim 10\%$).

As a further step, we strive to (i) extend our IP microscopy to the excited-state case, since the probing depends only on the phonon motions; (ii) reveal the NA effects on nonlinear phonon dynamics and IP in more general systems and phonon modes, esp. in experiments.

For the IP probing in excited states, as shown in Fig. S3 [50], with the electron excitation increasing, both the harmonic ω and anharmonic α decrease, indicating a softening of phonon energy originating from the electron-phonon coupling in excited state caused by the nonequilibrium electron distribution. The results also show that the phase transitions barrier is modulated by ~ 0.6 eV (~ 7000 K) under a ~ 0.04 V/Å laser field. The modulation of Young's modulus Y and TEC can be even more significant in excited graphene. As shown in Fig. S5 [50], the nonequilibrium carriers can weaken both the intrinsic elasticity and thermal expansion. Taking the laser field ~ 0.04 V/Å as an example, the Y and TEC are modulated by $\sim 5\%$ and $\sim 27\%$, respectively, proving an effective manipulation on material properties by photoexcitation.

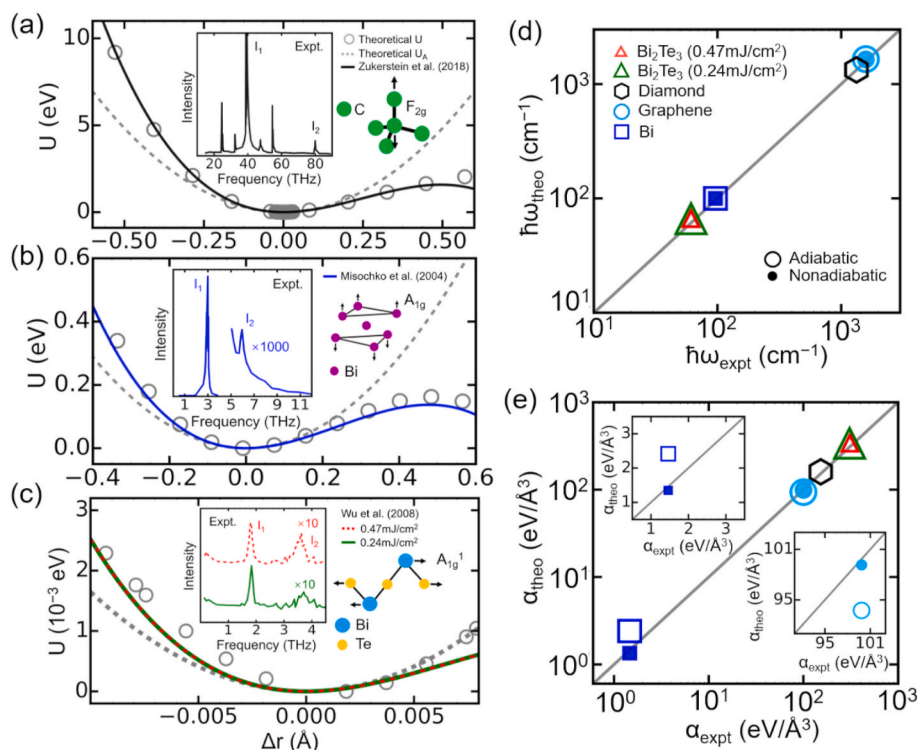


Fig. 4. The interatomic potential U as a function of phonon amplitude Δr reconstructed from the POS in the pump-probe experiments in diamond [33] (a), metal Bi [34] (b) and Bi_2Te_3 [35] (c), respectively. The grey circles and dash lines label the theoretical results of U and U_A , respectively [50]. The insets show the POS of transient reflectivity measured by experiments and the atomic patterns of the different phonon modes. (d) The phonon frequency ω of the harmonic potential term U_H from theoretical calculations compared to experiment measured ones. (e) The coefficient α of the anharmonic potential term U_{AH} from theoretical calculations compared to experiment measured ones. The open and solid circles label the results with ABO approximation (adiabatic) and NA corrections (nonadiabatic), respectively. The grey lines are the 1:1 ratios.

For NA effects in more general systems, in Fig. 4(a–c), for F_{2g} phonons in diamond [33], A_{1g} phonons in metal Bi [34] and A_{1g}^1 phonons in Bi_2Te_3 [35], we use the coherent POS (the insets in Fig. 4(a–c)) obtained from pump-probe experiments (the POS is proportional to Fourier transforms of the time-dependent transient reflectivity [29,33,]) to reconstruct the effective IP and study the NA effects on it.

More details are shown in Fig. 4(d) and (e). Both the phonon frequency ω in U_H and coefficient α in U_{AH} show consistency between theory and experiment. For graphene and metal Bi which have strong NA effects, the α in NA framework is in a closer agreement with the experimental value, indicating that the NA corrections exist ubiquitously for the accurate description of IP in many-body systems. Compared to graphene ($\sim 7.54\%$ NA corrections on α), the NA effects on anharmonic potential parts in metal Bi are even more significant, which can correct nearly half of the value ($\Delta\alpha/\alpha \sim 44.6\%$).

The good agreements demonstrate the robustness and universality of our approach, which is effective both for theory and experiment. Beside the NA effects investigation, the direct and accurate IP probing itself may broaden the measurement technology to include a direct access to the chemical, lattice and topological properties of matters. For example, during the phase transitions between graphite and diamond [60,61], the evidence in Raman spectrum for diamondene, which is a 2D diamond material with outstanding properties on ferromagnetic semiconductor, is provided recently [62]. The spectroscopic detection of diamondene requires a high resolution. One of the reasons is that the energy of the F_{2g}/E_{2g} mode in diamond and graphite/graphene is very close, $\omega_{\text{graphene}}/\omega_{\text{diamond}} \sim 1.18$ as shown in Fig. 4. However, considering the total IP structure including the anharmonic part, the ratio of coefficient α between graphene and diamond is $\alpha_{\text{graphene}}/\alpha_{\text{diamond}} \sim 1.6$, which is more distinguishable. The results suggest that accurate probing of the effective IP may help us to detect the mixed phases more easily.

In conclusion, based on our advanced IP probing method beyond the harmonic, adiabatic and equilibrium approximation, we reveal the significant NA effects on coherent phonons and effective IP. The NA effects strongly modulate the anharmonic potential term (up to $\sim 50\%$) and adjust the phase transition barriers. As a consequence, the

corresponding nonlinear phonon dynamics, phonon-mode-resolved Young's modulus and TEC are impacted. Our study demonstrates the nonadiabaticity has more universal and important effects than we thought before on the various properties of many-body system. Moreover, the IP probing developed in our work can be further combined with other technologies including the field-resolved spectroscopy [63] and the time-resolved techniques. All of the results are keys to dynamic investigations of the intrinsic elastic/thermal properties, phase transitions/reactions in materials, which would facilitate rational design of catalysts, materials and drugs.

Credit author statement

Shi-Qi Hu: Conceptualization, Methodology, Validation, Formal analysis, Investigation, Data Curation, Writing - Original Draft, **Da-Qiang Chen:** Methodology, Software, **Sheng-Jie Zhang:** Validation, Formal analysis, **Xin-Bao Liu:** Methodology, Formal analysis, **Sheng Meng:** Conceptualization, Writing - Review & Editing, Supervision, Project administration, Funding acquisition.

Declaration of competing interest

The authors declare that they have no known competing financial interests or personal relationships that could have appeared to influence the work reported in this paper.

Data availability

The data that support the findings of this study are available from the corresponding author upon reasonable request.

Acknowledgements

We acknowledge financial support from MOST (grant 2021YFA1400200), NSFC (grants 12025407, 11934003, 91850120, 11774328) and CAS (XDB330301).

Appendix A. Supplementary data

Supplementary data to this article can be found online at <https://doi.org/10.1016/j.mtphys.2022.100790>.

References

- [1] T.F. Nova, Profile A.S. Disa, M. Fechner, A. Cavalleri, *Science* 364 (2019) 6445.
- [2] R. Mankowsky, A. von Hoegen, M. Först, A. Cavalleri, *Phys. Rev. Lett.* 118 (2017): 197601.
- [3] Y. Saito, T. Nojima, Y. Iwasa, *Nat. Commun.* 9 (2018) 778.
- [4] A. Cavalleri, *Contemp. Phys.* 59 (2018) 31.
- [5] T. Frigge, B. Hafke, T. Witte, B. Krenzer, C. Streubühr, A. Samad Syed, V. Mikšić Trontl, I. Avigo, P. Zhou, M. Ligges, D. von der Linde, U. Bovensiepen, M. Horn-von Hoegen, S. Wippermann, A. Lücke, S. Sanna, U. Gerstmann, W.G. Schmidt, *Nature* 544 (2017) 207.
- [6] J. Maklar, Y.W. Windsor, C.W. Nicholson, M. Puppini, P. Walmsley, V. Esposito, M. Porer, J. Rittmann, D. Leuenberger, M. Kubli, M. Savoini, E. Abreu, S. L. Johnson, P. Beaud, G. Ingold, U. Staub, I.R. Fisher, R. Ernstorfer, M. Wolf, L. Rettig, *Nat. Commun.* 12 (2021) 2499.
- [7] S. Hammes-Schiffer, A.V. Soudackov, *J. Phys. Chem. B* 112 (2008): 14108.
- [8] E.G. Lewars, *Computational Chemistry*, third ed., Springer, 2016.
- [9] Potential Energy Surfaces <https://chem.libretexts.org/go/page/20275> (accessed Jul 4, 2021).
- [10] M. Born, J.R. Oppenheimer, *Ann. Phys.* 84 (1927) 457.
- [11] J.M. Ziman, *Electrons and Phonons*, Oxford Univ. Press, Oxford, 1960.
- [12] G. Grimvall, *The Electron-Phonon Interaction in Metals*, North-Holland, Amsterdam, 1981.
- [13] M. Lazzeri, F. Mauri, *Phys. Rev. Lett.* 97 (2006): 266407.
- [14] S. Pisana, M. Lazzeri, C. Casiraghi, K.S. Novoselov, A.K. Geim, A.C. Ferrari, F. Mauri, *Nat. Mater.* 6 (2007) 198.
- [15] A.M. Saitta, M. Lazzeri, M. Calandra, F. Mauri, *Phys. Rev. Lett.* 100 (2008): 226401.
- [16] F. Caruso, M. Hoesch, P. Achatz, J. Serrano, M. Krisch, E. Bustarret, F. Giustino, *Phys. Rev. Lett.* 119 (2017): 017001.
- [17] G.D. Barmparis, Y.S. Puzryev, X.-G. Zhang, S.T. Pantelides, *Phys. Rev. B* 92 (2015): 214111.
- [18] A. Alkauskas, Q. Yan, C.G. Van de Walle, *Phys. Rev. B* 90 (2014): 075202.
- [19] T. Kampfrath, K. Tanaka, K.A. Nelson, *Nat. Photonics* 7 (2013) 680.
- [20] R. Mankowsky, A. Subedi, M. Först, S.O. Mariager, M. Chollet, H.T. Lemke, J. S. Robinson, J.M. Glowia, M.P. Minitti, A. Frano, M. Fechner, N.A. Spaldin, T. Loew, B. Keimer, A. Georges, A. Cavalleri, *Nature* 516 (2014) 71.
- [21] M. Först, C. Manzoni, S. Kaiser, Y. Tomioka, Y. Tokura, R. Merlin, A. Cavalleri, *Nat. Phys.* 7 (2011) 854.
- [22] S.W. Teitelbaum, T. Henighan, Y. Huang, H. Liu, M.P. Jiang, D. Zhu, M. Chollet, T. Sato, Éamonn D. Murray, S. Fahy, S. Mahony, T.P. Bailey, C. Uher, M. Trigo, D. A. Reis, *Phys. Rev. Lett.* 121 (2018): 125901.
- [23] J. Ding, J.L. Niedziela, D. Bansal, J. Wang, X. He, A.F. May, G. Ehlers, D. L. Abernathy, A. Said, A. Alatas, Y. Ren, G. Arya, O. Delaire, *Nat. Acad. Sci. USA* 117 (2020) 3930.
- [24] J. Ding, T. Lanigan-Atkins, M. Calderón-Cueva, A. Banerjee, D.L. Abernathy, A. Said, A. Zevalkin, O. Delaire, *Sci. Adv.* 7 (2021): eabg1449.
- [25] T. Tadano, S. Tsuneyuki, *Phys. Rev. Lett.* 120 (2018): 105901.
- [26] A. Cavalleri, C.W. Siders, F.L.H. Brown, D.M. Leitner, C. Tóth, J.A. Squier, C.P. J. Barty, K.R. Wilson, K. Sokolowski-Tinten, M. Horn von Hoegen, D. von der Linde, M. Kammler, *Phys. Rev. Lett.* 85 (2000) 586.
- [27] Eeuwe S. Zijlstra, Jessica Walkenhorst, Martin E. Garcia, *Phys. Rev. Lett.* 101 (2008): 135701.
- [28] Sunghyun Kim, Samantha N. Hood, Aron Walsh, *Phys. Rev. B* 100 (2019): 041202.
- [29] K.G. Nakamura, K. Ohya, H. Takahashi, T. Tsuruta, H. Sasaki, S. Uozumi, K. Norimatsu, M. Kitajima, Y. Shikano, Y. Kayanuma, *Phys. Rev. B* 94 (2016): 024303.
- [30] H. Katsuki, J.C. Delagnes, K. Hosaka, K. Ishioka, H. Chiba, E.S. Zijlstra, M.E. Garcia, H. Takahashi, K. Watanabe, M. Kitajima, Y. Matsumoto, K.G. Nakamura, K. Ohmori, *Nat. Commun.* 4 (2013) 2801.
- [31] O.V. Misochko, J. Flock, T. Dekorsy, *Phys. Rev. B* 91 (2015): 174303.
- [32] N. Ratcliff, L. Hallett, B.R. Ortiz, S.D. Wilson, J.W. Harter, *Phys. Rev. Mater.* 5 (2021) L111801.
- [33] M. Zukerstein, M. Kozák, F. Trojánek, P. Malý, *Diam. Relat. Mater.* 90 (2018) 202.
- [34] O.V. Misochko, Muneaki Hase, K. Ishioka, M. Kitajima, *Phys. Rev. Lett.* 92 (2004): 197401.
- [35] A.Q. Wu, X. Xu, *Appl. Phys. Lett.* 92 (2008): 011108.
- [36] A. von Hoegen, R. Mankowsky, M. Fechner, M. Först, A. Cavalleri, *Nature* 555 (2018) 79.
- [37] C. Lian, S.J. Zhang, S.Q. Hu, M.X. Guan, S. Meng, *Nat. Commun.* 11 (2020) 43.
- [38] J. Zhang, C. Lian, M.X. Guan, W. Ma, H.X. Fu, H. Guo, S. Meng, *Nano Lett.* 19 (2019) 6027.
- [39] A.W. Tsena, R. Hovden, D. Wang, Y.D. Kim, J. Okamoto, K.A. Spothb, Y. Liuf, W. Luf, Y. Sunf, J.C. Honed, L.F. Kourkoutis, P. Kima, A.N. Pasupathy, *Nat. Acad. Sci. USA* 112 (2015): 15054.
- [40] D. Novko, *Commun. Phys.* 3 (2020) 30.
- [41] L. Li, X. Chang, X. Lin, Z.-J. Zhao, J. Gong, *Chem. Soc. Rev.* 49 (2020) 8156.
- [42] S. Mitchell, J. Pérez-Ramírez, *Nat. Commun.* 11 (2020) 4302.
- [43] B. Dereka, Q. Yu, N.H.C. Lewis, W.B. Carpenter, J.M. Bowman, A. Tokmakoff, *Science* 371 (2021) 160.
- [44] C. Zhu, Q. Shi, S. Feng, D. Du, Y. Lin, *ACS Energy Lett.* 3 (2018) 1713.
- [45] J. Guan, Z. Duan, F. Zhang, S.D. Kelly, R. Si, M. Dupuis, Q. Huang, J.Q. Chen, C. Tang, C. Li, *Nat Catal* 1 (2018) 870.
- [46] J. Hulva, M. Meier, R. Bliem, Z. Jakub, F. Kraushofer, M. Schmid, U. Diebold, C. Franchini, G.S. Parkinson, *Science* 371 (2021) 375.
- [47] S. Meng, E. Kaxiras, *J. Chem. Phys.* 129 (2008): 054110.
- [48] C. Lian, S. Hu, M. Guan, S. Meng, *J. Chem. Phys.* 149 (2018): 154104.
- [49] C. Lian, M. Guan, S. Hu, J. Zhang, S. Meng, *Adv. Theory Simul.* 1 (2018): 1800055.
- [50] See Supplemental Materials for the Details.
- [51] H. Lakhota, H.Y. Kim, M. Zhan, S. Hu, S. Meng, E. Goulielmakis, *Nature* 583 (2020) 55.
- [52] S. Hüller, J. Meyer-ter-Vehn, *Phys. Rev. A* 48 (1993) 3906.
- [53] Péter Kálmán, Thomas Brabec, *Phys. Rev. A* 52 (R) (1995) R21.
- [54] Y. Zhao, L. Du, W. Yang, C. Shen, J. Tang, X. Li, Y. Chu, J. Tian, K. Watanabe, T. Taniguchi, R. Yang, D. Shi, Z. Sun, G. Zhang, *Phys. Rev. B* 102 (2020): 165415.
- [55] G. Froehlicher, S. Berciaud, *Phys. Rev. B* 91 (2015): 205413.
- [56] J. Lin, L. Guo, Q. Huang, Y. Jia, K. Li, X. Lai, X. Chen, *Phys. Rev. B* 83 (2011): 125430.
- [57] I. Efthimiopoulos, S. Mayanna, E. Stavrou, A. Torode, Y. Wang, *J. Phys. Chem. C* 124 (2020) 4835.
- [58] C. Lee, X. Wei, J.W. Kysar, J. Hone, *Science* 321 (2008) 385.
- [59] P.R. Shaina, L. George, V. Yadav, M. Jaiswal, *J. Phys. Condens. Matter* 28 (2016): 085301.
- [60] A.P.M. Barboza, M.H.D. Guimaraes, D.V.P. Massote, L.C. Campos, N.M.B. Neto, L. G. Cancado, R.G. Lacerda, H. Chacham, M.S.C. Mazzoni, B.R.A. Neves, *Adv. Mat.* 23 (2011) 3014.
- [61] W.L. Mao, H.-k. Mao, P.J. Eng, T.P. Trainor, M. Newville, C.-c. Kao, D.L. Heinz, J. Shu, Y. Meng, R.J. Hemley, *Science* 302 (2003) 425.
- [62] L.G.P. Martins, M.J.S. Matos, A.R. Paschoal, P.T.C. Freire, N.F. Andrade, A. L. Aguiar, J. Kong, B.R.A. Neves, A.B. de Oliveira, M.S.C. Mazzoni, A.G.S. Filho, L. G. Cançado, *Nat. Commun.* 8 (2017) 96.
- [63] I. Pupeza, M. Huber, M. Trubetskov, W. Schweinberger, S.A. Hussain, C. Hofer, K. Fritsch, M. Poetzlberger, L. Vamos, E. Fill, T. Amotchkina, K.V. Kepesidis, A. Apolonski, N. Karpowicz, V. Pervak, O. Pronin, F. Fleischmann, A. Zezeer, M. Zigmán, F. Krausz, *Nature* 577 (2020) 52.